

# Critical parameters for the partial coalescence of a droplet

T. Gilet,<sup>1,\*</sup> K. Mulleners,<sup>1</sup> J.P. Lecomte,<sup>2</sup> N. Vandewalle,<sup>1</sup> and S. Dorbolo<sup>1,†</sup>

<sup>1</sup> GRASP, Physics Department B5,  
University of Liège, B-4000 Liège, Belgium

<sup>2</sup>Dow Corning S.A.  
Parc Industriel-Zone C  
B-7180 Seneffe - Belgium

(Dated: December 2, 2024)

The partial coalescence of a droplet onto a planar liquid/liquid interface is investigated theoretically by using a dimensional analysis. It mainly depends on the Bond number (gravity vs. surface tension), the Ohnesorge numbers (viscosity in both fluids in contact vs. surface tension) and the density relative difference. An experimental work on 2000 coalescence events is made in order to study the impact of viscosities and gravity on the coalescence process. Global quantities such as the available surface energy of the droplet has been measured during the coalescence. The surface energy is converted into kinetic energy at a constant rate that is independent of the coalescence outcome. The ratio between the daughter droplet size and the mother droplet size is investigated as a function of the dimensionless numbers. Theoretical models are proposed to fit experimental data. The asymmetrical behavior when liquids are inverted indicates that the viscous dissipation is different in both fluids. In the surrounding fluid, the capillary waves are damped during their travel from the bottom to the top of the droplet. Inside the droplet, the capillary waves are mainly damped during their creation at the bottom of the droplet. This unexplored damping mechanism is most probably achieved by the way of the vortex ring that is sometimes observed below the droplet during coalescence. Finally, according to the present theoretical models, predictions are made about the main features of partial coalescence for many couples of immiscible fluids. The maximum number of steps in the cascade has been found to be equal to 11. That could be obtained for an interface between mercury and a non-viscous immiscible liquid.

PACS numbers: 47.55.df, 47.55.D-, 47.55.db, 47.61.Ne, 47.85.lk

Keywords: Droplet physics, Partial Coalescence, Surface-tension-driven flows

## I. INTRODUCTION

Liquid droplets are more and more studied in the framework of microfluidic applications. Indeed, they allow to manipulate and transport very small quantities of liquids. Droplets coalescence is probably the most convenient way to mix liquids in microdevices without any power supply [1, 2]. Both control and reproducibility of the droplet sizes are therefore very important. For instance, one of the main difficulties encountered is to obtain a single small droplet, with a typical size lower than 100  $\mu\text{m}$ . Such a challenge is also present when dealing with the petrol injection in car motors. The smaller the droplets are, the more efficient the combustion is [3]. The partial coalescence is a suitable way to achieve such a goal since it progressively empties a droplet (see Fig.1).

In order to investigate partial coalescence, Charles and Mason [4] have studied a system composed by two immiscible fluids 1 and 2 of different densities (fluid 1 is heavier than fluid 2). This experiment is schematically represented on Fig.2. A thick layer of the lighter fluid 2 is placed over the bulk of fluid 1. A millimetric droplet of fluid 1 is then dropped over the system. It crosses the

fluid 2 layer and stays on the interface between fluid 1 and fluid 2 for a while depending on the viscosity of 2. Suddenly, the droplet coalesces. In given conditions that will be discussed, the droplet experiences a partial coalescence. A smaller droplet remains above the 1/2 interface. The process may occur several times, like a cascade: it is possible to get as much as six partial coalescences before the final total one. Note that this experiment is totally equivalent to a droplet of fluid 1 (lighter than fluid 2) coming up through fluid 2, when apparent gravity (gravity + buoyancy forces) is considered.

Charles and Mason attempted to explain the occurrence of partial coalescence by considering the ratio of dynamical viscosities in both fluids. But this only parameter is not enough to fully understand partial coalescence mechanisms. This experiment was studied in 1993 by Leblanc [5]. He was interested in the stability of emulsions. Indeed, partial coalescence considerably slows down the gravity-driven phase separation of two immiscible liquids, for instance when dealing with petrol demulsification. Leblanc identified every important parameter for a partial coalescence prediction, but his work remained unpublished. In 2000, Thoroddsen and Takehara [6] studied this phenomenon in more details for an air/water interface. Same conclusions as Leblanc emerged concerning the impact of viscosity on the flow. More recently, in 2006, Blanchette and Bigioni [7] have explained the mechanism of pinch-off in partial coales-

---

\*Electronic address: Tristan.Gilet@ulg.ac.be

†URL: <http://www.grasp.ulg.ac.be>

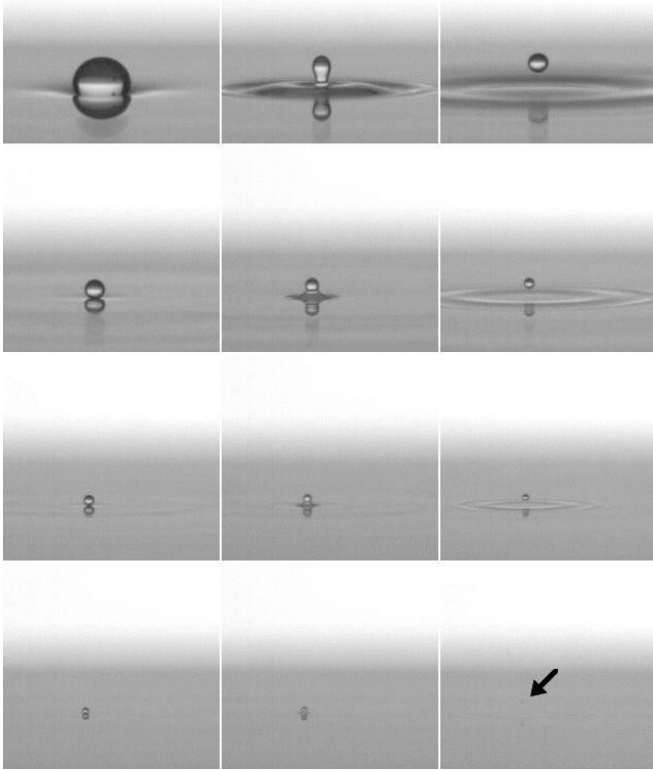


FIG. 1: A cascade of five partial coalescences of a water+soap droplet surrounded by air.

cence by using a subtle combination of both experimental and numerical techniques.

Little is known about microflows occurring during the coalescence process. First, traditional experimental techniques are difficult to be applied at droplet scale. However, PIV experiments on droplet coalescence were made by Mohamed-Kassim and Longmire [8]. Unfortunately, the droplet was too large to allow partial coalescence. The simplest way to get experimental information about microflows is to observe the interface position, as in [9] for instance. On a numerical point of view, free surface flows with changing topology (such as coalescence, breakdown and pinch-off) are really difficult and expensive to compute. More often, drastic simplifications are made. The flow is assumed to be potential (no vorticity) [10], or the fluid 2 is replaced by vacuum [7, 10]. Despite these difficulties, a lot of information have already been collected about microflows in a coalescence process.

The present paper is composed of two parts. First, an original dimensional analysis provides a complete and self-consistent picture of the partial coalescence process. Second, an experimental study is made over more than 2000 coalescence events, with various initial droplet sizes, viscosities and densities of both fluids. Using image processing, global variables such as the available potential surface energy are recorded during the coalescence pro-

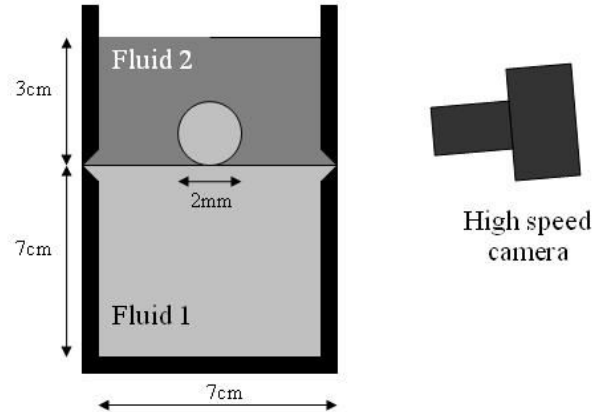


FIG. 2: Experimental setup: A container is filled with two immiscible fluids. A droplet of fluid 1 is falling through fluid 2, before coalescing with the fluid 1 bulk phase. The same experiment can be conducted when fluid 1 is lighter than fluid 2 (the droplet is going up).

cess. Their evolution analysis raise new questions and new challenges. A first step is made in the elaboration of the law that predicts the final droplet radius as a function of the initial one and of the physical properties of both fluids.

## II. DIMENSIONAL ANALYSIS

### A. Relevant dimensionless numbers

Once the thin film of fluid 2 below the droplet is broken, the dynamics of partial coalescence is macroscopically governed by only three kinds of forces: interfacial tension, gravity and viscosity forces in both fluids. There are seven macroscopic parameters: surface tension  $\sigma$ , densities  $\rho_1$  and  $\rho_2$ , kinematic viscosities  $\nu_1$  and  $\nu_2$ , gravity acceleration  $g$  and the initial droplet radius  $R_i$  ( $i = 1, 2$ ). According to the  $\pi$ -theorem (Vaschy-Buckingham), it is possible to build only four independent dimensionless numbers. Three of them are derived from the ratio of the characteristic time scales of the different forces. The capillary time is given by

$$\tau_\sigma = \sqrt{\frac{\rho_m R^3}{\sigma}} \quad (1)$$

where  $\rho_m$  is defined as the mean density  $\frac{\rho_1 + \rho_2}{2}$ . The gravity time is given by

$$\tau_g = \sqrt{\frac{R}{g'}} \quad (2)$$

( $g'$  is the apparent gravity experienced by the droplet), and the viscosity times by

$$\tau_{\nu 1/2} = \frac{R^2}{\nu_{1/2}} \quad (3)$$

The Bond number can be built

$$Bo = \frac{(\rho_1 - \rho_2)gR_i^2}{\sigma} \quad (4)$$

(gravity vs. surface tension), and the two Ohnesorge numbers

$$Oh_{1/2} = \frac{\nu_{1/2}\sqrt{\rho_m}}{\sqrt{\sigma R_i}} \quad (5)$$

(viscosity in fluids 1 and 2 vs. surface tension). The last dimensionless number can be the relative difference of density

$$\Delta\rho = \frac{\rho_1 - \rho_2}{\rho_1 + \rho_2} \quad (6)$$

Ideally, any dimensionless quantity can be expressed as a function of these four parameters, especially the ratio  $\Psi$  between the daughter droplet radius and the mother droplet radius

$$\frac{R_f}{R_i} = \Psi\left(Bo, Oh_1, Oh_2, \Delta\rho\right) \quad (7)$$

As Dooley et al. [11] or Thoroddsen and Takehara [6] have shown, the partial coalescence process is scaled by the capillary time. The surface tension has to be the main force for partial coalescence to occur. In other words, an auto-similar process is only possible when one force is dominant (the surface tension). That means that there is no natural length scale related to the balance of two forces.

For large droplets, gravity is known to be as important as surface tension. Therefore, gravity significantly accelerates the emptying of the mother droplet [5, 7]. The ratio  $\Psi$  is monotonically decreasing with  $Bo$ , and a critical Bond number  $Bo_c(Oh_1, Oh_2, \Delta\rho)$  exists for which  $\Psi = 0$  for any larger  $Bo$  than  $Bo_c$ : coalescence becomes total.

As shown by Blanchette and Bigioni [7], the partial coalescence process is mainly due to the convergence of capillary waves at the top of the droplet. These waves are generated at the beginning of the coalescence, by the receding interface below the droplet. The viscosity forces in both fluids, mainly present for smallest droplets, damp these capillary waves and inhibit the partial coalescence [5, 6, 7]. The ratio  $\Psi$  also monotonically decreases with both Ohnesorge numbers. Critical Ohnesorges numbers  $Oh_{1c}$  and  $Oh_{2c}$  may be defined; beyond which coalescence becomes total.

On the other hand, when the Bond (resp. Ohnesorge) number is much smaller than the critical Bond (resp.

Ohnesorge) number, gravity (resp. viscosity) can be considered as negligible. The  $\Psi$  function does not depend on  $Bo$  (resp.  $Oh$ ) anymore. For droplets with negligible Bond and Ohnesorge numbers,  $\Psi$  is equal to a constant  $\Psi_0$ . More precisely,  $\Psi_0$  only depends on  $\Delta\rho$ , the relative difference of inertial effects generated by the interfacial tension in both fluids. The process becomes auto-similar, since the densities do not change between two successive partial coalescences.

The previous dimensional analysis is correct when the droplet is at rest at the beginning of the coalescence. The radius is the only key parameter to describe the droplet. Such an hypothesis is true when microflows due to the previous droplet fall are damped out. The timescale of these flows can be roughly estimated as the time needed for the thin film of fluid 2 to be drained out. When this time is much larger than the capillary time, the initial microflows can be considered as negligible compared to the microflows generated by the coalescence process. This condition have to be checked for each experiment of coalescence.

Obviously, the film drainage time is shorter for a droplet surrounded by a gaz than for a droplet surrounded by a liquid. Therefore, it is easier to work with a liquid/liquid interface as evidenced by Mohammed-Kassim and Longmire [8]. Such an argument can explain why partial coalescence is observed with a water+soap/air interface, and not for a water/air interface. Considering pure water + air, hydrogen bonds cause a premature break down of the thin air film. The condition on initial microflows is not satisfied. The addition of surfactant allows partial coalescence because surfactant acts like a shield for hydrogen bonds. Besides, a rigid wall forms and the water cannot be entrained by air drainage. The time of drainage is then enhanced [5]. As a consequence, surfactant avoids premature breakdown. Since the coalescence is always total with pure water in air, it seems that initial microflows tend to enhance the droplet emptying, and to inhibit the partial coalescence.

The coalescence of a droplet on a planar interface is similar to the coalescence of two droplets with different radii. The planar case is obtained by setting the radius of the second droplet to infinity. Therefore, a lot of results introduced when tackling with the droplet-droplet coalescence are also verified in the planar case.

Now, the different stages of a coalescence process will be described in the light of this dimensional analysis.

## B. The initial stages

The film rupture usually occurs where the film is the thinnest. This latter is off-center, as it was shown experimentally by Hartland [12] and theoretically by Jones and Wilson [13]. This off-centering effect is mainly due to the presence of a surrounding fluid, which generates an overpressure at the center while drained out.

When the film is broken, it quickly opens due to high

pressure gradients created by surface tension near the hole (curvature is inversely proportional to film thickness). Eggers, Lister and Stone [14] have solved the problem of film ejection for low Reynolds numbers (viscosity dominated process) when the hole is initially not too much off-center. They found that the radius of the hole  $r_h$  obeys to the law

$$r_h \sim t \log t \quad (8)$$

Thoroddsen et al. [9] have shown that such hypothesis were never satisfied for common fluids, since the rupture is usually off-center and the surrounding fluid not viscous enough.

Aarts et al. [15] have experimentally studied droplets in very viscous surrounding fluid, and with a very low surface tension (inertial effects can be neglected). They have shown that the logarithmic contribution of Eq.(8) is not observed.

When inertia is dominant compared to viscosity, Eggers et al. [14] have proposed the following scaling law

$$r_h \sim \left( \frac{\sigma R}{\rho_1} \right)^{1/4} t^{1/2} \quad (9)$$

This law is based on a balance between inertia and surface tension; the biggest curvature is given by  $R/r_h^2$ . It is possible to rewrite this equation with the capillary time

$$\left( \frac{r_h}{R} \right)^2 \sim \frac{t}{\tau_\sigma} \quad (10)$$

This power-law fits well with experimental data, as shown by Menchaca et al. [16], Wu et al. [1] or Thoroddsen et al. [9]. Despite the absence of a surrounding fluid, numerical simulations of Duchemin et al. [10] give the same agreement with Eq.(9). However, the proportionality constant, of the order of unity, varies from one author to the other one.

Thoroddsen, Takehara and Etoh [9] have proposed another law, also based on a balance between surface tension and inertia

$$\frac{dr_m}{dt} = C \sqrt{\frac{\sigma}{\rho_1} \left( \frac{1}{\delta(r_m)} - \frac{1}{r_m} \right)} \quad (11)$$

where  $\delta(r_m)$  is the film thickness at a distance  $r_m$  from the axis.  $C$  is approximately 0.8 and does not seem to vary with droplet size and interface curvature. However,  $C$  decreases when the droplet is compressed on the interface, and when viscosity becomes important.

During the retraction, a part of the bulk phase of fluid 1 comes up into the droplet, as shown by Brown and Hanson [17]. They observed a slightly colored daughter droplet when using a colorless mother droplet on a colored bath. This upward movement is depicted in [11].

### C. Vorticity creation

The coalescence of two droplets with different radii is known as one of the best ways to mix micro-quantities of fluid [18]: since there is a difference in Laplace pressure between both droplets, the smallest one empties into the biggest one. During the coalescence, a powerful vortex ring penetrates into the big droplet, easily demonstrated with a milk droplet on a surface of water. This vortex considerably enhances the mixing process. This vortex may also be present in the coalescence between a droplet and a planar interface.

Anilkumar et al. [18] and Shankar et al. [19] have measured and modelled the penetration depth of this vortex. Cresswell and Morton [20] have described in details the way vorticity is generated. In ideal partial coalescence conditions (viscosity and gravity forces negligible compared to surface forces at the scale of the droplet - axisymmetry), vorticity cannot be created inside bulk phases. Therefore, it has to be generated at the interface. The authors have shown that vorticity appears when there is a tangential flow near a curved interface (here when the broken film retracts). The boundary layer associated to this tangential flow can experience a separation, and vorticity is therefore released in the bulk phase as a big mushroom-shaped vortex ring. Separation occurs when the boundary layer is thin enough. Cresswell and Morton have proposed a criterium to quantify this argument. Before separation, the smallest radius of curvature of the hole in the broken film  $r_2$  have to satisfy

$$\frac{r_2 V}{\nu_1} < 4\pi \quad (12)$$

Considering the result of Cresswell et al. with a velocity  $V$  equal to the capillary velocity  $V_\sigma = \sqrt{\sigma/\rho_m R}$ , we obtain that the separation becomes possible when

$$\frac{r_2}{R} > 4\pi Oh_1 \quad (13)$$

The Ohnesorge number is a determinant parameter in this problem. Supposing that the biggest value for  $r_2$  (where separation is still possible) is  $\alpha R$ ,  $\alpha < 1$ , we conclude that when the fluid is too viscous ( $4\pi Oh_1 > \alpha$ ), the separation cannot occur and vorticity is not released in the bulk phase. There are no vortex rings and the droplet experiences a blob: The fluid of the coalescing droplet spreads on the interface instead of penetrating in depth. Experimentally, Shankar et al. [19] have obtained a critical Ohnesorge number  $Oh_{1v}$  for vortex release about 0.025. Therefore,  $\alpha$  is about 0.3 and the vortex leaves the interface when  $r_2 = 0.3R$ .

Cresswell and Morton [20] have also shown that the Weber number  $We$  (quantifying the kinetic energy of the falling droplet vs. surface energy) has a deep impact on vortex ring creation. This latter only occurs for  $We < 8$ .

Anilkumar et al. [18] have checked experimentally their theoretical prediction about the penetration depth

of the vortex  $L$  for small Ohnesorge numbers ( $Oh_1 \ll Oh_{1v}$ )

$$\frac{L}{R} \simeq \frac{K}{\sqrt{Oh_1}} \quad (14)$$

According to these authors, the proportionality constant  $K$  does not depend on  $Oh_2$  since no change was observed while the viscosity of fluid 2 was set from  $2cP$  to  $200cP$ .

Considering a droplet-droplet coalescence as in [18], vortex rings are generated when the ratio between the biggest and the smallest droplet radius is large enough: no vortex ring is observed when the two droplet have the same size. However, Thoroddsen et al. [9] have shown that in this case vorticity is probably produced in the same way, but is not released. Indeed, the constant  $C$  in their hole expansion model is independent on the radii ratio : no less energy is lost during the hole expansion when vortex rings cannot appear. Vorticity remains concentrated near the coalescing droplet.

#### D. Capillary waves and pinch-off

During a partial coalescence process, the emptying droplet takes a column shape, and then experiences a pinch-off that leads to the formation of the daughter droplet. Charles and Mason [4] have suggested this pinch-off was due to a Rayleigh-Plateau instability.

Recently, Blanchette and Bigioni [7] have shown that this hypothesis was wrong. They have solved Navier-Stokes equations for a coalescing water droplet surrounded by air. When the top of the droplet reaches its maximum height, they stop the numerical simulation, set velocities and pressure perturbations to zero and restart the computation. The coalescence, nominally partial, was observed to be total with this flow reset. The pinch-off cannot be due to a Rayleigh-Plateau instability.

Leblanc [5], Thoroddsen et al. [6] and Mohamed-Kassim et al. [8] have already noted the existence of capillary waves generated at the bottom of the droplet after the film break-down. A part of these waves propagates far away, on the planar interface. The other part climbs over the droplet and converges at the top.

According to Blanchette [7], such a convergence greatly deforms the droplet and delays its coalescence, the horizontal collapse (the pinch-off) can occur before. Gravity balances this delay by accelerating the emptying of the droplet. In other words, too much gravity leads to a total coalescence. Viscosities of both fluids damp the capillary waves, the convergence effect is reduced and coalescence can also become total. The precise role played by viscosities in the capillary waves damping will be detailed in this paper.

After the pinch-off, the daughter droplet recovers its spherical shape while it is ejected upward. Recent experimental work by Honey et al. [21] analyses the maximum height and the restitution coefficient of this bouncing for a water/air interface. It seems that the maximal height is

minimal for a Bond number of 0.1. For smaller and larger droplets, the height increases. The restitution coefficient seems to be approximately constant (slightly decreasing) and approximately 0.22.

### III. EXPERIMENTAL SETUP

Our experimental set-up consists in a glass vessel which is opened at the top. This container is half filled with the fluid 1. A centimetric layer of fluid 2 is then gently poured over the fluid 1 (see schematic view on Fig.2). A horizontal guide groove is dug in the vertical borders of the container to reduce the meniscus at the oil/water interface (and in order to get a quasi-planar interface), as interface curvature is known to modify the drainage time. Besides, according to Blanchette [7], it can also influence the result of partial coalescence. A syringe is used to create a small droplet of fluid 1, colored by methylene blue for visualization purpose. By changing the needle diameter, the initial droplet radius  $R_0$  can be changed. Between each experiment, the set-up is washed with acetone to avoid interface contamination.

The cascade of partial coalescences is studied using a set of different silicon oils for the fluid 2 (Trimethylsilyl terminated polydimethylsiloxane, under the tradename Dow Corning 200 fluid). Their kinematic viscosity  $\nu_2$  can be easily tuned from  $\nu_2=0.65$  to  $100$  cSt. Mixtures are made in order to obtain intermediate viscosities. The fluid 1 is made of a mixture of water and alcohol (glycerol or ethanol). The kinematic viscosity  $\nu_1$  may be modified by the alcohol/water ratio. Densities are also changed (see Table I). The interfacial tension is approximately  $30$  mN/m for any oil/water interfaces. We have explored the different regimes of partial and total coalescence (autosimilarity, influence of high viscosities and high apparent gravity).

In order to ensure that no significant microflows are present at the beginning of the coalescence process, the experiments for which the film drainage time is less than one second are rejected. The vessel is big enough to avoid parasite reflections of capillary waves on the walls during the coalescence.

A fast video recorder (Redlake Motion Pro) is placed near the surface. A slight tilt (less than  $10^\circ$ ) is needed to see the bottom of the droplet, since the interface is curved by the weight of the droplet. Movies of the coalescence have been recorded up to 2000 frames per second, as seen on the snapshot of Fig.3. The pixel size is about  $30 \mu\text{m}$ . About 2000 coalescence events have been recorded. The droplet/camera distance is roughly constant. Distances on the picture are measured with a relative error less than 10%. Since this error on distances is constant during a single coalescence experiment, ratios of distances (such as the radii ratio  $\Psi$ ) are characterized by an error significantly smaller than forecasted.

Initial and final radii are measured for every experiment. In order to get information about the partial co-

Liquid	$\rho(\text{kg}/\text{m}^3)$	$\nu(\text{cSt})$
W	1000	0.893
87.5%W + 12.5%G	1030	1.16
75%W + 25%G	1063	1.64
62.5%W + 37.5%G	1093	2.65
50%W + 50%G	1127	4.74
25%W + 75%G	1195	30.1
90%W + 10%E	983	1.35
80%W + 20%E	969	1.82
70%W + 30%E	954	2.23
60%W + 40%E	934	2.47
DC-0.65cSt	760	0.65
DC-1.5cSt	830	1.5
DC-5cSt	915	5
DC-10cSt	934	10
DC-50cSt	960	50
DC-100cSt	965	100
80%DC-10cSt + 20%DC-100cSt	940	19.5
60%DC-10cSt + 40%DC-100cSt	946	30.4
40%DC-10cSt + 60%DC-100cSt	953	46.4
20%DC-10cSt + 80%DC-100cSt	959	69.7

TABLE I: Experimental setup: Fluid properties (G=Glycerol, E=Ethanol, W=water, DC=Dow Corning 200 oil).

alescence process, the whole interface is tracked on each snapshot for 300 experiments. Of course, we suppose that the interface (and even the whole flow) is axisymmetric. It is then possible to estimate global measurements such as the volume above the interface, or the surface potential energy for instance.

An original, highly robust and threshold-less interface detection method has been developed. Note that the reflected light can be detected as a part of the interface, generating high discontinuities in interface shape. These discontinuities are detected and deleted in the post-processing.

## IV. RESULTS AND DISCUSSION

### A. The global variables evolution

In order to get more information about the partial coalescence process, we have measured global quantities associated to the detected interface on each experimental image: the volume  $V$  of fluid 1 above the mean interface level, the available surface potential energy  $SPE$  (as in [9]), the available gravity potential energy (proportional to the mass centre position  $MCP$  of fluid 1 above the mean interface level) and the height of the top  $h$  (i.e. the interface vertical position on the symmetry axis, as studied in [8, 16]).

The available surface energy, normalized by its initial value, is plotted as a function of time on Fig.4(a). Results of three experiments with different surrounding viscosities are presented: a partial coalescence ( $Oh_2 \ll Oh_{2c}$ ), an attenuated partial coalescence ( $Oh_2 \lesssim Oh_{2c}$ ) and a total coalescence ( $Oh_2 > Oh_{2c}$ ). Figure 4(a) shows that the coalescence process is scaled by the capillary time, since the surface energy decrease is roughly independent

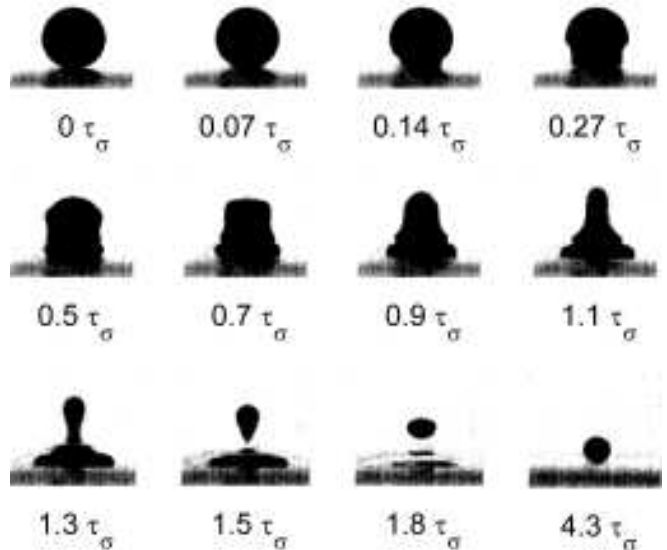


FIG. 3: Experimental images of a detailed partial coalescence, from left to right and from up to down. The whole process is scaled by the capillary time  $\tau_\sigma$ .

of the coalescence issue. Besides, during the whole coalescence process, the decrease is remarkably linear. Therefore, we can assess that surface potential energy is converted into kinetic energy at a constant rate. This rate does not seem to depend on  $Oh_2$ , and corresponds to a 40%-decrease in surface energy during the capillary time. Such a decrease in surface energy was already observed when dealing with the initial hole opening ( $r_h \sim t^{1/2}$ ), as seen previously. We can see that the pinch-off (second discontinuity) occurs between  $1.4\tau_\sigma$  and  $1.8\tau_\sigma$  after the coalescence beginning (first discontinuity).

The volume  $V$  of the droplet above the mean interface level can be seen as a function of time on Fig.4(b). The droplet starts to significantly empty at approximately  $t = 0.5\tau_\sigma$ . As seen on the plot, it is possible to correctly fit data by the following law

$$\frac{V(t)}{V(t=0)} = 1 - C_V \left( \frac{t}{\tau_\sigma} \right)^3 \quad (15)$$

According to the fitting, the coefficient  $C_V$  is approximately 0.2, and experiences a slight increase with  $Bo$ . Indeed, on Fig.4(b), the Bond number is higher for the partial coalescence experiment than for the total one. Therefore, gravity enhances the droplet emptying. The flow rate  $Q$  through the mean interface level can be deduced by differentiate Eq.15.

$$\frac{Q\tau_\sigma}{V(t=0)} = 3C_V \left( \frac{t}{\tau_\sigma} \right)^2 \quad (16)$$

The time evolution of the vertical position  $MCP$  of the mass centre of the droplet is shown on Fig.4(c). It has

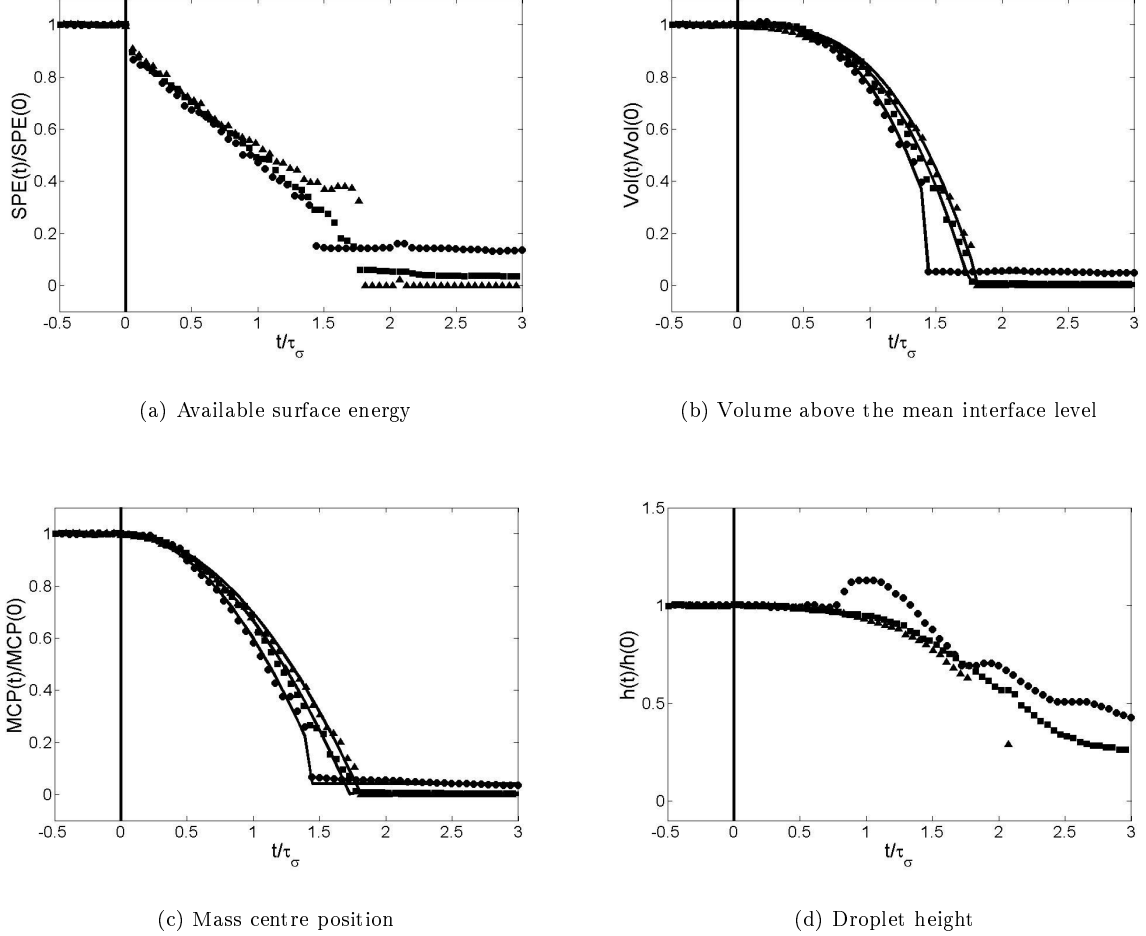


FIG. 4: Evolution of the global quantities for an autosimilar partial coalescence ( $\bullet$  -  $Oh_2 \ll Oh_{2c}$ ), an attenuated partial coalescence ( $\blacksquare$  -  $Oh_2 \lesssim Oh_{2c}$ ), and a total coalescence ( $\blacktriangle$  -  $Oh_2 > Oh_{2c}$ ).

a more pronounced decrease than the volume. Indeed, the droplet is larger on the bottom than on the top. The quantity  $MCP$  can be fitted by the law

$$\frac{MCP(t)}{MCP(0)} = 1 - C_{MC} \left( \frac{t}{\tau_\sigma} \right)^2 \quad (17)$$

with  $C_{MC} \simeq 0.3$ . As for the volume,  $C_{MC}$  increases with the Bond number.

Figure 4(d) shows the evolution of the droplet height (i.e. the distance between the top of the droplet and the mean interface level). First, this height is constant since only the bottom of the droplet moves. When the capillary waves are not too damped (partial coalescence), they converge at the top, and the height increases of about 15% to reach a maximum. On Fig.5, the maximum height  $h_{max}$  normalized by the initial height  $h_0$  is plotted with respect  $Oh_2$ . We can see that this maximum decreases as the damping (i.e.  $Oh_2$ ) increases. The decrease can be approximated by a decreasing exponential

$$\frac{h_{max} - h_0}{h_0} \simeq 0.15e^{-\frac{Oh_2}{Oh_{2w}}} \quad (18)$$

$Oh_{2w}$  is the Ohnesorge number in the ambient fluid for which the waves are significantly damped at the top. It is found to be equal to about 0.04.

When capillary waves are damped enough, i.e.  $Oh_2 > Oh_{2w}$  - partial attenuated and total coalescences, the height monotonically decreases. Note that, as it will be shown in the next section, the critical Ohnesorge number for the damping of waves  $Oh_{2w}$  is smaller than  $Oh_{2c}$ . Therefore, it is possible to get partial coalescence (attenuated) with highly damped capillary waves.

For undamped waves, the propagation time  $t_{CW}$  can be estimated from measurements. It is the time until the first motion at the top can be observed. On Fig.6, it can be seen that this time greatly decreases with the Bond number. For large Bond numbers, Mohamed-Kassim and Longmire [8] obtained a propagation time approximately equal to 0.6 capillary time units.

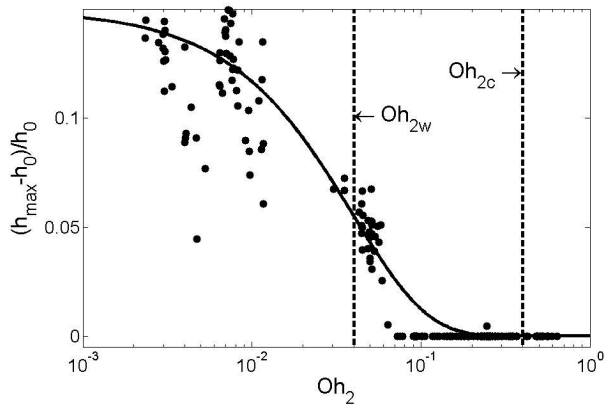


FIG. 5: Maximum droplet height normalized by the initial height vs. Ohnesorge 2 number. The fitting law is given by Eq.(18).

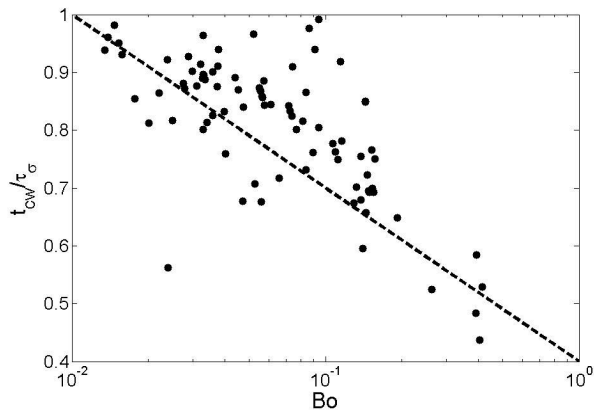


FIG. 6: Propagation time vs.  $Bo$ . The dashed line is a guide for the eyes.

The dispersion relationship of surface-gravity waves on a planar interface between two semi-infinite media is given by

$$(\omega\tau_\sigma)^2 = \frac{l}{2} (l^2 + Bo) \quad (19)$$

where  $l$  is the angular momentum  $kR$ ,  $k$  the wave number and  $R$  the initial droplet radius. For  $Bo < 1$ , the influence of  $Bo$  on this dispersion relationship is negligible compared to  $l^2$ . The group velocity is *a priori* unaffected by the Bond number, and this cannot explain the observed decrease in the propagation time. Another explanation could reside in the flattening of the droplet on the interface before the coalescence when  $Bo \lesssim Bo_c$ .

### B. The $\Psi$ law

In this section, the ratio between the daughter droplet radius and the mother droplet radius (the  $\Psi$  function) is

investigated.

#### 1. Asymptotic regime

Thanks to the dimensional analysis (see section II), we have shown that for negligible  $Bo$ ,  $Oh_1$  and  $Oh_2$  (surface tension is the only dominant force),  $\Psi$  depends only on the density relative difference.

As shown by Blanchette [7], capillary waves that travel along the droplet are responsible for the pinch-off process. Therefore, we need to understand the behavior of such waves to assess about their impact, i.e. the final radius. Considering axisymmetric and irrotational perturbations of an ideal incompressible droplet without gravity, it is possible to find the dispersion relationship of capillary waves on a spherical interface

$$(\omega_l\tau_\sigma)^2 = \frac{l(l^2 - 1)(l + 2)}{2l + 1 + \Delta\rho} \quad (20)$$

where  $\tau_\sigma$  is the capillary time  $\sqrt{\rho_m R^3/\sigma}$ , and the interface is given by

$$R(t, \theta) = R_0 + \sum_l \tilde{r}_l P_l(\cos\theta) \cos\omega_l t \quad (21)$$

where  $\tilde{r}_l$  is the perturbation amplitude component associated to  $P_l$ , the Legendre polynomial of degree  $l$ .

Assuming relatively small wavelengths, we can assess that  $l = kR \gg 1$  and the dispersion relationship becomes

$$(\omega_l\tau_\sigma)^2 = \frac{l^3}{2} \quad (22)$$

Since this relation is independent on  $\Delta\rho$ , a difference in density between both fluids does not generate any significant delay in the wave propagation to the top.

This suggests that the dependance of  $\Psi$  on the density relative difference is weak and may be first neglected. Therefore, in the asymptotic regime, experimental results show that one has

$$\Psi = \Psi_0 = cst. \simeq 0.5 \quad (23)$$

#### 2. Influence of the Bond number

The figure 7 shows the observed influence of the Bond number on  $\Psi$ . Data from Charles and Mason [4] are incorporated for comparison purposes (triangles). For small Bond numbers, the asymptotic regime is obtained. As noted in the dimensional analysis, an increase in the Bond number results in a decrease in  $\Psi$ , and there is a critical Bond number  $Bo_c$  about 0.7 for which  $\Psi$  becomes zero. The coalescence is total.

Supposing that the gravity enhances the emptying of the droplet by removing an additional part  $\Delta V$  of the

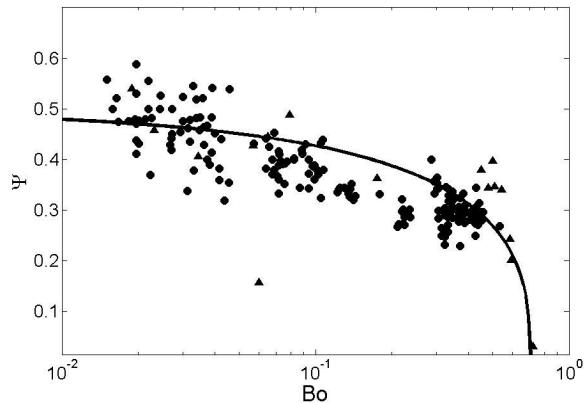


FIG. 7: Bond influence on the radius ratio  $\Psi$ . Model predictions vs. experimental results: our measurements ( $\bullet$ ) and Charles & Mason [4] measurements ( $\blacktriangle$ ). The solid line corresponds to the fitting law, given by Eq.(28).

mother droplet initial volume  $V_i$ , the volume  $V_f$  of the daughter droplet is given by

$$\frac{V_f}{V_i} \simeq \Psi_0^3 - \frac{\Delta V}{V_i} \quad (24)$$

The mean flow rate due to gravity is roughly equal to

$$Q_g = \frac{V_i}{\tau_g} \quad (25)$$

Since the partial coalescence duration is scaled on  $\tau_\sigma$ , we can assess that

$$Q_g \simeq \frac{\Delta V}{\tau_\sigma} \quad (26)$$

The Bond number is defined as the square of the ratio between the capillary time and the gravity time. Considering all these equations, we can infer the following law for  $\Psi$  dependence on Bond number

$$\frac{R_f}{R_i} = \Psi \simeq \sqrt[3]{\Psi_0^3 - C\sqrt{Bo}} \quad (27)$$

where  $C$  is a positive proportionality constant. The ratio  $\Psi$  has to vanish when  $Bo \rightarrow Bo_c$ . The constant  $C$  can be deduced, resulting in the following law

$$\frac{\Psi}{\Psi_0} \simeq \sqrt[3]{1 - \sqrt{\frac{Bo}{Bo_c}}} \quad (28)$$

meaning that  $\Psi$  reaches  $\Psi_0$  when gravity effects are negligible ( $Bo \ll Bo_c$ ). As seen on Fig.7, there is a good agreement between experimental data and Eq.(28), with  $\Psi_0 \simeq 0.5$  and  $Bo_c \simeq 0.7$ .

### 3. Influence of the Ohnesorge numbers

On Fig.8(a) and 8(b), the dependences of  $\Psi$  on Ohnesorge numbers is plotted. Viscous dissipation in fluid

2 leads to a smooth decreasing of  $\Psi$  with  $Oh_2$ , starting from the asymptotic regime. The critical Ohnesorge for partial coalescence  $Oh_{2c}$  is about 0.4, which is 10 times greater than  $Oh_{2w}$ , the critical Ohnesorge for wave damping at the top of the droplet. Leblanc have observed  $Oh_{2c} \simeq 0.32$ , which is quite in accordance with our results.

The behavior with increasing  $Oh_1$  is totally different: the decrease of  $\Psi$  is very sharp. The ratio  $\Psi$  immediately vanishes to zero when  $Oh_1 > Oh_{1c} \simeq 0.02$ . This critical value was already obtained by Blanchette [7] (a  $\sqrt{2}$  factor is needed to have the same definition of the Ohnesorge number), and thirteen years ago by Leblanc [5] (who found 0.024).

In order to take both viscosities into account, Leblanc suggested that the critical parameter for partial coalescence occurrence is a linear combination of both Ohnesorge numbers. Partial coalescence takes place when

$$Oh_1 + 0.057Oh_2 < 0.02 \quad (29)$$

This law is compared to experimental results on figure 9. The discrepancy between the model and the data indicates that the dissipative mechanisms are different in both fluids.

It is possible to build a simple model to describe the behavior of  $\Psi$  as a function of  $Oh_2$ . As noted by Blanchette [7], viscosity acts on  $\Psi$  by damping the capillary waves. This damping of the wave amplitude is modelled by Eq.(18), mentioned in the previous section.

Suppose that the ratio  $\Psi$  also experiences an exponential decrease when  $Oh_2$  increases. The exponential coefficient has to be related to the critical Ohnesorge  $Oh_{2c}$ . The decrease has to be shifted since the coalescence becomes total ( $\Psi = 0$ ) for a finite  $Oh_2$ . One has

$$\frac{\Psi}{\Psi_0} \simeq C_1 e^{\frac{Oh_2}{Oh_{2c}}} + C_2 \quad (30)$$

$C_1$  and  $C_2$  are constants that can be found by imposing that  $\Psi$  tends to  $\Psi_0$  when  $Oh_2 \ll Oh_{2c}$  and vanishes when  $Oh_2 \rightarrow Oh_{2c}$ . The following relation can be inferred

$$\frac{\Psi}{\Psi_0} = \frac{e^{\left(1 - \frac{Oh_2}{Oh_{2c}}\right)} - 1}{e - 1} \quad (31)$$

This model seems to capture the main quantitative features of experimental data, as shown on Fig.8(b). However, as it can be seen on Fig.8(a), it fails in predicting the behavior of  $\Psi$  when  $Oh_1$  is varying: another model has to be proposed for describing the behaviour with respect to fluid 1 (see next section).

For negligible  $Oh_1$  values, we can try to combine models for  $Bo$  and  $Oh_2$  influences on  $\Psi$ . Let us consider  $\Psi_1$  the  $\Psi$  function when  $Bo$  and  $Oh_1$  are negligible.

$$\frac{\Psi_1}{\Psi_0} = \frac{e^{\left(1 - \frac{Oh_2}{Oh_{2c}}\right)} - 1}{e - 1} \quad (32)$$

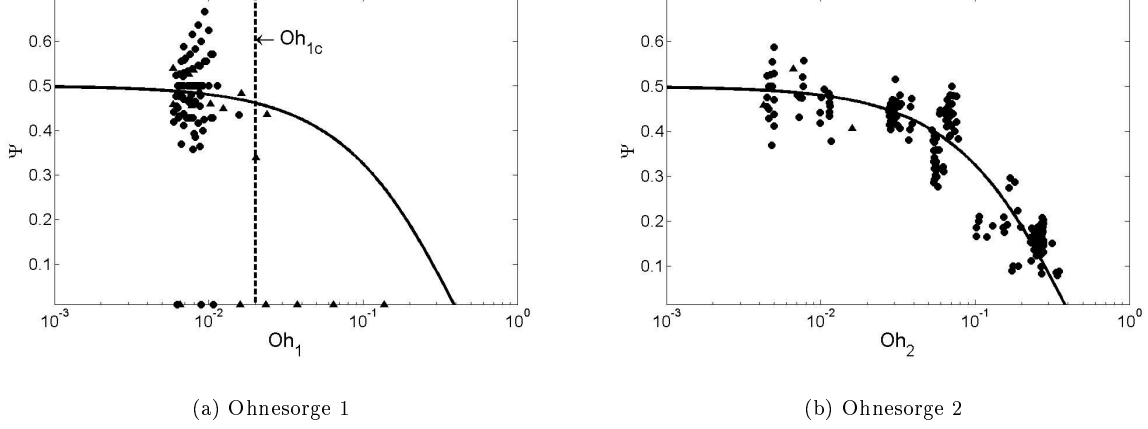


FIG. 8: Ohnesorge influence on the radius ratio  $\Psi$ . Model predictions vs. experimental results: our measurements ( $\bullet$ ) and Charles & Mason [4] measurements ( $\blacktriangle$ ). The fitting law is given by Eq.31.

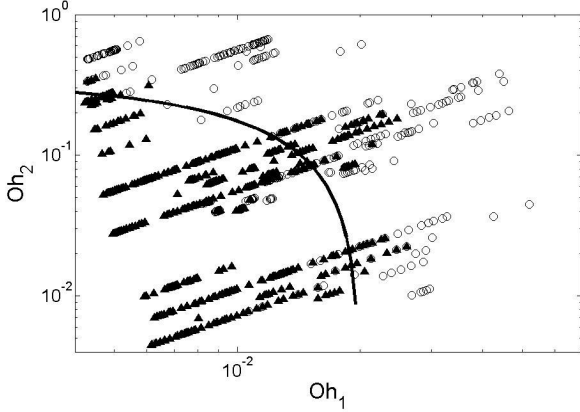


FIG. 9: Phase plan  $Oh_1/Oh_2$ : experimental results. Total coalescence ( $\circ$ ) vs. partial coalescence ( $\blacktriangle$ ). The solid line corresponds to the linear relationship (29).

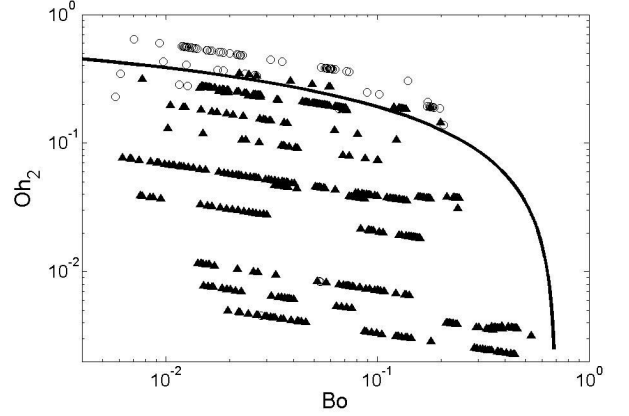


FIG. 10: Phase plan  $Bo/Oh_2$ : experimental results. Total coalescence ( $\circ$ ) vs. partial coalescence ( $\blacktriangle$ ). The fitting law is given by Eq.(34).

$\Psi_1$  can be injected instead of  $\Psi_0$  in Eq.(27) to take the influence of viscosity into account in the Bond law. This leads to the following result

$$\frac{\Psi(Bo, Oh_2)}{\Psi_0} = \sqrt[3]{\left(\frac{\Psi_1(Oh_2)}{\Psi_0}\right)^3 - \sqrt{\frac{Bo}{Bo_c(Oh_2 \rightarrow 0)}}} \quad (33)$$

Partial coalescence becomes total when  $Bo$  is equal to  $Bo_c$ , with

$$\frac{Bo_c}{Bo_c(Oh_2 \rightarrow 0)} = \left(\frac{\Psi_1}{\Psi_0}\right)^6 \quad (34)$$

Figure 10 indicates when coalescence is total or partial, for different  $Bo$  and  $Oh_2$  values. The boundary between these behaviours is well-captured by Eq.(34).

#### 4. Viscous dissipations in both fluids

According to the linear wave theory, the particular geometry of the interface has no effects on the capillary waves damping. Indeed, the velocity field is given by

$$\vec{v} \simeq \begin{cases} \alpha(\theta, \omega, l) \left(\frac{r}{R}\right)^{l-1} & \text{in fluid 1} \\ \alpha(\theta, \omega, l) \left(\frac{r}{R}\right)^{-l-2} & \text{in fluid 2} \end{cases} \quad (35)$$

The energy dissipation rate in both fluids is given by

$$D = \int_V \mu \frac{\partial v_i}{\partial x_j} \left( \frac{\partial v_i}{\partial x_j} + \frac{\partial v_j}{\partial x_i} \right) r^2 \sin \theta dr d\theta d\phi \quad (36)$$

When viscosities are similar, it is straight forward to show that the energy dissipation rate is similar in both fluids,

for every  $l$ -mode. Therefore, for the same viscosities, waves are not especially more damped by the fluid in the droplet than by the ambient fluid during their propagation from bottom to top.

But why the critical Ohnesorge in fluid 2 is about 20 times higher than the critical Ohnesorge in fluid 1? Why fluid 1 is more able to damp capillary waves than fluid 2?

To address these questions, it is necessary to focus on the time  $t_M$  needed by capillary waves to reach the top of the droplet. This time is given by

$$\frac{t_M}{\tau_\sigma} \simeq \frac{\pi R}{v_g \tau_\sigma} \simeq \frac{4\pi}{3\sqrt{2}} l^{-1/2} \text{ when } l \geq 3 \quad (37)$$

This normalized time is observed to be about 0.8, according to the experimental data on Fig.6. A simple numerical simulation was made to confirm this result. We considered the propagation of a small gaussian perturbation Eq.(38) from the bottom to the top of a droplet, according to the dispersion relationship Eq.(20).

$$R(\theta, t = 0) = R_0 + Ae^{-\frac{(\theta - \theta_0)^2}{\pi/300}} \quad (38)$$

The maximum amplitude, due to convergence on the top, was observed after  $0.77\tau_\sigma$ . This agrees with the experimental results.

Eq.(37) gives propagation times lower than the capillary time when  $l \gtrsim 10$ . This means that the nine first modes are still on the way when the maximum of convergence is observed at the top. Therefore, the convergence cannot be due to these modes. Indeed, deleting the 9 first modes from the initial perturbation does not impair the convergence quality.

According to Blanchette [7], the viscous dissipation in fluid 1 is given by the ratio of the propagation characteristic time  $t_M$  and the dissipation characteristic time  $1/D$ . In fluid 1,

$$D_1 t_M \simeq (2\nu_1 k^2) t_M \simeq \frac{8\pi}{3\sqrt{2}} Oh_1 l^{3/2} \quad (39)$$

The authors specify that the dissipation is of the order of unity when the coalescence becomes total

$$\frac{8\pi}{3\sqrt{2}} Oh_{1c} l^{3/2} \simeq 1 \quad (40)$$

Considering  $Oh_{1c} \simeq 0.025$ , we find  $l \simeq 3 - 4$ , negligible modes for the convergence process. Setting  $l = 15$  gives  $D_1 t_M (Oh_1 = Oh_{1c}) \simeq 8.6$  and  $D_2 t_M (Oh_2 = Oh_{2c}) \simeq 138$  instead of unity. Since the propagation time is well-estimated, it means that the dissipation estimation is not correct.

Concerning fluid 2, we have shown that partial coalescence can exist when the waves are totally damped on the top of the droplet (this corresponds to an attenuated partial coalescence). Indeed, the critical Ohnesorge for wave damping ( $Oh_{2w} \simeq 0.04$ ) is about ten times

less than the critical Ohnesorge for partial coalescence ( $Oh_{2c} \simeq 0.4$ ). Therefore, it is reasonable to think that  $D_2 t_M (Oh_2 = Oh_{2c}) \sim 10$ .

The  $l$ -mode corresponds to an half-wavelength about  $\pi R/l$ . Observing the interface movements, we can infer that the length scale of velocity gradients is probably not the half-wavelength with  $l > 10$ . Indeed, the superposition of wave modes creates a wave packet with a significantly greater characteristic length scale (empirically about  $\pi R/4$ , as seen on Fig.3). The viscous dissipation has to be computed according to this new length scale, based on  $l = l_d \simeq 4$ .

Thus, we can assess that, similarly to Eq.39,

$$D_2 t_M \simeq 2 \frac{\nu_2}{R^2} l_d^2 \cdot \frac{4\pi}{3\sqrt{2}} \tau_\sigma l^{-1/2} \simeq \frac{8\pi}{3\sqrt{2}} Oh_2 l_d^2 l^{-1/2} \quad (41)$$

Considering  $l = 15$ ,  $l_d = 4$  and  $D_2 t_M = 10$ , we can find the critical Ohnesorge for partial coalescence, about 0.4. This new estimation of the wave damping can explain viscosity effects in fluid 2 on the partial coalescence.

Concerning fluid 1, another mechanism have to dissipate 20 times more energy than during the wave propagation. According to Fig.8(a), the transition is brutal, which suggests an on/off mechanism.

Let us suppose that this mechanism is the vortex ring. This seems plausible since vortices suddenly disappear when the separation of the boundary layer (an on/off event) becomes impossible, i.e. for  $Oh_1 \gtrsim 0.02$ . This limit is exactly the critical Ohnesorge in fluid 1 for partial coalescence.

Another argument can be given: As suggested by Thoroddsen [9], vortices are always created during the initial stages of a coalescence process between two droplets. This operation needs the same amount of energy, not depending of the size of the droplets. This independence suggests that it is also applicable to the coalescence of a droplet with a planar interface. What differs is the fact that these vortices are able or not to separate from the interface. When the droplets have a similar size or when the fluid 1 is too viscous, the vortices cannot separate. As a consequence, they will further dissipate the kinetic energy just released by the interface instead of dissipating the kinetic energy in the bulk phase, faraway. If vortices are able, they separate when  $r_2 \simeq 0.3R$ , as shown previously by using Cresswell and Morton [20] results. The most surprising is the following experimental fact observed by Leblanc [5]: Partial coalescence can be inhibited by placing a horizontal solid board just below the interface, typically at a distance of  $0.3R$ . In this configuration, vortex rings cannot escape and the dissipation is fully effective in the droplet : coalescence is total.

Therefore, we can conclude that the vortex ring is most probably the main dissipative mechanism responsible for total coalescences in viscous fluids 1. It damps the capillary waves during their creation, at the bottom of the droplet. Further experimental studies could confirm this theory.

Finally, considering Cresswell and Morton's work [20], we can assess that partial coalescence is inhibited when the droplet comes to the interface with a high velocity (Weber number  $We > 8$ ). Indeed, the vortex will not be able to separate and viscous dissipation will be too important to allow a partial coalescence.

### 5. Number and size of daughter droplets

It is possible to estimate the maximum number of daughter droplets for a couple of fluids starting from their physical properties (available in [22] and [23] for instance). The maximum droplet size (limited by gravity - Eq.4) has a radius of the order of

$$R_M \simeq \sqrt{\frac{\sigma B o_c}{2\rho_m \Delta \rho g}} \quad (42)$$

while the minimum droplet radius (viscosity limited - Eq.5) is of the order of

$$R_m \simeq \max_{i=1,2} \left\{ \frac{\rho_m \nu_i^2}{\sigma O h_{ci}^2} \right\} \quad (43)$$

Supposing that  $\Psi \simeq 0.5$  during the whole cascade, the upper bound of the possibles numbers of steps in the cascade  $N$  is given by

$$\frac{\max(R_{m1}, R_{m2})}{R_M} \simeq (0.5)^N \quad (44)$$

When  $N = 1$ , the coalescence is total.

The capillary time can be estimated for the largest and the smallest droplet. Besides, we have to ensure that this time is always very short compared to the drainage time (when the droplet stays at rest on a thin film of fluid 2). When the fluid 2 has a dynamical viscosity significantly smaller than the fluid 1, the film drainage does not entrain the fluid 1 (neither in the droplet, nor in the bulk phase). The Reynolds' model [5], based on the lubrication equation, is of application. The lifetime  $LT$  is given by

$$LT \approx \frac{3\mu_2 R^4}{4\pi g(\rho_1 - \rho_2)h_c^2} \quad (45)$$

$h_c$  is the critical film thickness, when the film breaks. When dynamical viscosities are similar, the film drainage entrains fluid 1, and the Reynolds'theory have to be replaced by Ivanov and Traykov's equation [24]

$$LT \approx \left( \frac{\rho_1 \mu_1 R^2}{32\pi^2 g^2 (\rho_1 - \rho_2)^2 h_c^2} \right)^{1/3} \quad (46)$$

This equation is used to provide a crude estimation of the lifetime of the droplets in Table II. Note that the drainage time is highly influenced by several factors: surfactant [5], electric fields [25], vibrations [26], and initial conditions among others.

Tables II and III give predicted orders of magnitude of  $R_M$ ,  $R_{m1}$ ,  $R_{m2}$ , the associated lifetimes and capillary times, and the number of steps  $N$  for different fluids 1. The fluid 2 is air (A), water (W) or mercury (M). When fluid 2 is heavier than fluid 1, the droplet crosses the interface from bottom to top. When the symbol \* is used, fluids 1 and 2 are inverted (for example a droplet of mercury surrounded by benzene instead of a droplet of benzene surrounded by mercury). The results in bold have been approximately checked experimentally (by Charles and Mason [4], Leblanc [5] or our results).

We can see in Tables II and III that, contrary to Thoroddsen's predictions [3], the coalescence of a mercury droplet surrounded by air is done in only 6 stages. The maximum number of cascade steps is obtained for a mercury droplet surrounded by a non-viscous liquid, such as acetone, benzene, heptane, chloroform or ether. No more than 11 stages will be observed in this case. The record could be broken by working with giant droplets in microgravity. Note that a 11-stage cascade is really hard to observe with a traditional optical instrumentation, since the smallest droplets have a radius of about 0.6 micrometers. Besides, these droplets have a lifetime about 0.5 milliseconds and they probably coalesce in less than 100 nanoseconds. The continuum media approach is usually valid. Indeed, when working with two liquids, the mean free path is clearly smaller than the last droplet, about 600 nanometers. And when working with a liquid surrounded by air, the air viscosity avoids droplets below 10 micrometers.

Note that a simple droplet of water surrounded by air coalesces in one step, because of the hydrogen bonds effect on the film drainage. Adding surfactant molecules can allow the partial coalescence. But since it decreases the surface tension, a soapy droplet will not experience a seven steps coalescence, as predicted in Tables II and III. We can also explain why a bubble of air always coalesces totally. The air is basically too viscous to give rise to a partial coalescence.

Data are not in agreement with our predictions concerning an aniline droplet surrounded by water. The aniline experiences as much as three partial coalescences, while our predictions state for a total coalescence. However, a vortex ring is observed and the dissipation can be avoided near the coalescing droplet. Therefore, the critical Ohnesorge  $Oh_{1c}$  for the vortex release seems to be significantly higher than 0.02 in this case. The reason is still unknown and needs further investigations.

## V. CONCLUSIONS

The partial coalescence has been investigated theoretically, by using a dimensional analysis. Ideally, partial coalescence only depends on four dimensionless parameters, the Bond number (gravity/surface tension), the Ohnesorge numbers in both fluids (viscosity/surface tension) and the density relative difference. The partial coales-

Name	Chemical Formula	Other Phase	$\rho_1$ ( $kg/m^3$ )	$\nu_1$ (cSt)	$\sigma$ (mN/m)	$R_M$ (mm)	$LT_M$ (s)	$\tau_{\sigma M}$ (ms)	$R_{m1}$ ( $\mu m$ )	$R_{m2}$ ( $\mu m$ )	$LT_m$ (ms)	$\tau_{\sigma m}$ ( $\mu s$ )	$N$
Acetic acid	$C_2H_4O_2$	A	1049	1.16	27.8	1.4	0.19	7.0	64	27	25	70	4
Acetone (25°C)	$C_3H_6O$	A	787	0.39	23.5	1.5	0.14	7.2	6.3	25	9.4	17	5
		M			390.0	1.5	0.022	7.7	6.9	$1.4e-3$	0.62	25	7
		M*					0.097		0.56	0.017	0.50	0.056	11
Aniline	$C_6H_7N$	A	1022	4.30	42.9	1.7	0.35	7.9	550	17	160	1.4e3	1
		W			6.1	4.4	8.5	120	7.6e3	1	12e3	2.7e5	1
		W*					5.1		410	19	1100	3400	3
Benzene	$C_6H_6$	A	879	0.74	28.9	1.5	0.18	7.4	21	22	10	12	6
		M			357	1.4	0.029	7.6	27	$1.5e-3$	21	20	5
		M*					0.09		0.61	0.068	0.54	0.068	11
		W			35.0	4.5	1.4	50	36	0.17	56	36	6
		W*					1.7		67	0.091	100	90	6
Carbon disulphide	$CS_2$	A	1263	0.30	32.3	1.4	0.12	7.0	4.3	28	9.2	21	5
Carbon tetrachloride	$CCl_4$	A	1594	0.61	27.0	1.1	0.12	6.4	10	39	12	41	4
		W			45.0	2.3	0.43	19	27	0.18	22	24	6
		W*					0.37		72	0.067	37	100	5
Chloroform	$CHCl_3$	A	1489	0.38	27.1	1.1	0.12	6.4	10	39	12	41	4
		W			28.0	2.0	0.36	19	16	0.28	15	14	6
		W*					0.38		110	0.041	56	250	4
		M			357.0	1.5	0.034	8.0	7.7	$1.6e-3$	1.0	3.1	7
		M*					0.099		0.64	0.019	0.57	0.074	11
Cyclohexane (25°C)	$C_6H_{12}$	W	773	1.15	41.1	3.6	0.83	32	71	0.11	61	89	5
		W*					0.91		43	0.18	47	41	6
DC200-0.65cSt (25°C)		A	761	0.65	15.9	1.2	0.15	6.6	25	36	14	34	5
		W			$\approx 30$	3	0.58	28	31	0.15	28	30	6
		W*					0.77		58	0.078	56	76	5
DC200-1.5cSt (25°C)		A	830	1.50	17.6	1.2	0.20	6.6	130	36	45	240	3
		W			$\approx 30$	3.5	1.1	37	17	0.15	150	390	4
		W*					1.1		60	0.43	72	82	5
DC200-10cSt (25°C)		A	934	10.0	20.1	1.2	0.37	6.7	5800	35	1000	6.8e4	1
		W			$\approx 30$	5.7	6.0	77	8100	0.16	7600	1.3e5	1
		W*					2.8		64	20	140	92	6
DC200-50cSt (25°C)		A	960	50.0	20.8	1.2	0.64	6.7	1.4e5	35	1.5e4	8.3e6	1
		W			$\approx 30$	7.3	17	110	2.0e5	0.16	1.6e5	1.7e7	1
		W*					4.6		65	510	780	2100	3

TABLE II: Theoretical prediction of cascades of partial coalescence events for different couples of fluids. Fluid 1 is given in the first column while fluid 2 is air (A), water (W) or mercury (M). When the symbol \* is used, fluids 1 and 2 are inverted.

Name	Chemical Formula	Other Phase	$\rho_1$ ( $kg/m^3$ )	$\nu_1$ ( $cSt$ )	$\sigma$ ( $mN/m$ )	$R_M$ ( $mm$ )	$LT_M$ ( $s$ )	$\tau_{\sigma M}$ ( $ms$ )	$R_{m1}$ ( $\mu m$ )	$R_{m2}$ ( $\mu m$ )	$LT_m$ ( $ms$ )	$\tau_{\sigma m}$ ( $\mu s$ )	$N$	
DC200-100cSt (25°C)		A	965	100	20.9	1.2	0.8	6.7	5.8e5	35	4.8e4	6.7e7	1	
		W			$\simeq 30$	<b>7.8</b>	25	<b>130</b>	8.2e5	0.16	5.5e5	1.3e8	1	
		W*					<b>5.3</b>			65	<b>2000</b>	2200	1.7e4	<b>1</b>
Di-ethyl ether	$C_4H_{10}O$	A	714	0.34	17.0	1.3	0.12	6.8	6.1	30	10	24	5	
		M			379.0	1.5	0.019	7.6	5.4	$1.4e-3$	0.47	1.7	8	
		M*					0.095		0.57	0.014	0.51	0.059	11	
		W			10.0	1.6	0.26	18	25	0.54	16	36	6	
		W*					0.47		210	0.062	120	920	2	
Dodecane	$C_{12}H_{26}$	W	750	1.80	47.0	<b>3.7</b>	0.9	30	<b>150</b>	0.12	110	250	4	
		W*					0.89		47	0.38	49	43	6	
Ethanol	$C_2H_6O$	A	789	1.52	22.8	1.4	0.22	7.2	100	25	37	130	3	
Ethyl acetate	$C_4H_8O_2$	A	925	0.49	23.6	1.4	0.14	6.9	12	28	11	21	5	
Formic acid	$CH_2O_2$	A	1220	1.32	37.13	1.5	0.21	7.3	71	23	28	77	4	
Glycerol	$C_3H_8O_3$	A	1261	1185	63.4	1.9	2.4	8.2	3.5e7	14	1.7e6	2.1e10	1	
		M			370.0	<b>1.5</b>	0.45	7.9	7.0e7	$1.5e-3$	5.9e5	8.3e10	1	
		M*					0.099		0.61	1.8e5	2400	1.0e7	<b>1</b>	
Mercury (25°C)	$Hg$	A	13546	0.11	486.1	1.6	0.099	7.6	0.46	20	5.3	10	6	
			13534	0.11	471	1.6	0.098	7.5	0.46	22	5.6	12	6	
Methanol	$CH_4O$	A	791	0.75	22.6	1.4	0.17	7.2	25	25	12	17	5	
n-Heptane	$C_7H_{16}$	M	684	0.72	379.0	1.5	0.024	7.6	25	$1.4e-3$	1.6	17	5	
		M*					0.095		0.57	0.062	0.51	0.059	11	
		W			51.0	<b>3.4</b>	0.51	25	22	0.10	17	13	7	
		W*					0.73		<b>41</b>	0.054	38	34	<b>6</b>	
n-Hexane	$C_6H_{14}$	A	659	0.58	18.4	1.4	0.16	7.1	15	26	11	17	5	
n-Octane	$C_8H_{18}$	A	703	0.78	21.8	1.5	0.18	7.3	24	23	12	15	5	
		W			51.0	3.5	0.56	27	25	0.10	21	16	7	
		W*					0.77		42	0.063	40	35	6	
Toluene	$C_7H_8$	A	867	0.67	28.4	1.5	0.17	7.4	17	22	10	13	6	
		W			28.0	<b>3.9</b>	1.1	44	38	0.21	52	43	6	
		W*					1.4		<b>83</b>	0.095	110	140	<b>5</b>	
Water (25°C)	$H_2O$	A	1000	1.00		2.3	0.26	9.0	17	9.8	10	6.0	7	
		A*						7.2e-3		3900	0.043	10	2.0e4	1
				0.89		72.0	2.3	0.25	9.0	14	11	8.3	4.3	7

TABLE III: Theoretical prediction of cascades of partial coalescence events for different couples of fluids. Fluid 1 is given in the first column while fluid 2 is air (A), water (W) or mercury (M). When the symbol \* is used, fluids 1 and 2 are inverted.

cence can occur only when the Bond and the Ohnesorge numbers are below critical values  $Bo_c$ ,  $Oh_{1c}$  and  $Oh_{2c}$ , since surface tension has to be the only dominant force. Otherwise, the coalescence is total. This approach was applied on a review of the different studies about microflows in a coalescence process.

An experimental work on 2000 coalescence events has been made in order to study the impact of viscosity and gravity on the coalescence process. The droplets were filmed and the images post-processed in order to determine the droplet radii, but also quantities such as the potential surface energy along any coalescence process. Surprisingly, it seems that this surface energy is converted into kinetic energy at a constant rate, that does not depend on the coalescence outcome. This observation has no explanation until now. The position of the top of the droplet was also investigated. It seems that partial coalescence is still possible when waves are fully damped when arriving to the top. The maximum of elevation was observed about 0.8 capillary time unit after the beginning of coalescence.

The  $\Psi$  law, which represents the ratio between the daughter and the mother droplet radii, has been investigated as a function of  $Bo$ ,  $Oh_1$  and  $Oh_2$ . When these numbers are small enough,  $\Psi$  becomes equal to approximately 0.5. Gravity is known to accelerate the emptying of the droplet, while viscosity damps the waves during their propagation. Simple models have been developed. They succeed in predicting the  $\Psi$  decreasing with increasing  $Bo$ , increasing  $Oh_2$  or a combination of both parameters. The critical Bond number is about 0.7, while the critical Ohnesorge number in fluid 2 is about 0.4: 10 times larger than the critical Ohnesorge for waves damping.

Blanchette and Bigioni [7] have shown that partial coalescence was due to the waves convergence on the top of the droplet. We have shown that only the  $l$ -modes upper than 10 are able to be on time for the convergence. But, contrary to Blanchette's thoughts, the viscous dissipation during capillary waves propagation is not scaled on these modes. It is scaled on the mean size of the wave

packet. Such assumptions allow us to correctly predict the critical Ohnesorge in fluid 2 for partial coalescence.

Viscosity dissipation is about twenty times more active in fluid 1 than in fluid 2, since the critical Ohnesorge number is about 0.02 in fluid 1. Another dissipation mechanism has been suspected. Besides, the  $\Psi$  function reaches zero without smooth transition, indicating that this mechanism can be turned on/off. Several arguments, based on previous works, suggest that the dissipation mechanism is played by the vortex ring. When it can separate, the energy dissipation in fluid 1 is negligible near the droplet and coalescence can be partial. When it cannot separate, the dissipation near the droplet is effective, capillary waves are damped during their creation and the coalescence becomes total.

Finally, a prediction of cascade features was made for a great number of different fluids. The record is probably a 11-step cascade, when using an interface between mercury and another non-viscous liquid. Such a cascade has not been observed for now. It would imply the use of advanced microscopy technique to observe the late stages of the cascade.

Although partial coalescence begins to be understood, many questions remain unexplored. The evolution of quantities such as the surface energy or the mass center position is unexplained at the moment. The exact influence of the density relative difference is unknown. Besides, there are many other factors that can influence the partial coalescence result: the interface curvature, a surfactant addition, electric fields, ...

### Acknowledgments

This work has been financially supported by Colgate-Palmolive Inc. The authors would like to thank especially Dow Corning S.A., Dr. G. Broze, Dr. H. Caps, Dr. M. Bawin, PhD Student S. Gabriel and S. Becco for their fruitful help. This work has been also supported by the contract ARC 02/07-293.

- 
- [1] M. Wu, T. Cubaud, and C-M. Ho, *Physics of Fluids* **16** (2004).
  - [2] H.A. Stone, A.D. Stroock, and A. Ajdari, *Annual Review on Fluid Mechanics* **36**, 381 (2004).
  - [3] S. Thoroddsen, *Nature Physics* **2**, 223 (2006).
  - [4] G.E. Charles and S.G. Mason, *Journal of Colloid Science* **15**, 105 (1960).
  - [5] Y. Leblanc, Ph.D. thesis, Université Paris VII (1993).
  - [6] S.T. Thoroddsen and K. Takehara, *Physics of Fluids* **12**, 1265 (2000).
  - [7] F. Blanchette and T.P. Bigioni, *Nature Physics* **2**, 1 (2006).
  - [8] Z. Mohamed-Kassim and E.K. Longmire, *Physics of fluids* **16**, 2170 (2004).
  - [9] S.T. Thoroddsen, K. Takehara, and T.G. Etoh, *Journal of Fluid Mechanics* **527**, 85 (2005).
  - [10] L. Duchemin, J. Eggers, and C. Josserand, *Journal of Fluid Mechanics* **487**, 167 (2003).
  - [11] B.S. Dooley, A.E. Warncke, M. Gharib, and G. Tryggvason, *Experiments in Fluids* **22**, 369 (1997).
  - [12] S. Hartland, *Trans. Inst. Chem. Eng.* **45** (1967).
  - [13] A.F. Jones and S.D.R. Wilson, *Journal of Fluid Mechanics* **87**, 263 (1978).
  - [14] J. Eggers, J.R. Lister, and H.A. Stone, *Journal of Fluid Mechanics* **401**, 293 (1999).
  - [15] D.G.A.L. Aarts, H.N.W. Lekkerkerker, H. Guo, G.H. Wegdam, and D. Bonn, *Physical Review Letters* **95**, 164503 (2005).
  - [16] A. Menchaca-Rocha, A. Martinez-Davalos, and R. Nunez, *Physical Review E* **63**, 046309 (2001).

- [17] C. Hanson and A.H. Brown, *Solvent Extraction Chemistry* **522** (1967).
- [18] A.V. Anilkumar, C.P. Lee, and T.G. Wang, *Physics of Fluids A* **3**, 2587 (1991).
- [19] P.N. Shankar and M. Kumar, *Physics of Fluids* **7**, 737 (1995).
- [20] R.W. Cresswell and B.R. Morton, *Physics of Fluids* **7**, 1363 (1995).
- [21] E.M. Honey and H.P. Kavehpour, *Physical Review E* **73**, 027301 (2006).
- [22] G.W.C. Kaye and T.H. Laby, *Tables of physical and chemical constants, and some mathematical functions* (Longman, 1973), 14th ed.
- [23] D. Lide, *Handbook of Chemistry and Physics* (CRC Press, 2005), 83rd ed.
- [24] I.B. Ivanov and T.T. Traykov, *International Journal of Multiphase Flow* **2**, 397 (1976).
- [25] J.S. Eow and M. Ghadiri, *Colloids and Surfaces A: Physicochemistry Engineering Aspects* **215**, 101 (2003).
- [26] Y. Couder, E. Fort, C.H. Gautier, and A. Boudaoud, *Physical Review Letters* **94**, 177801 (2005).